NJC

New Journal of Chemistry

A journal for new directions in chemistry

# Accepted Manuscript

This article can be cited before page numbers have been issued, to do this please use: Q. Zhou, L. Jia, F. Du, X. Dong, W. Sun, L. Wang and G. Chen, *New J. Chem.*, 2020, DOI: 10.1039/C9NJ04713A.

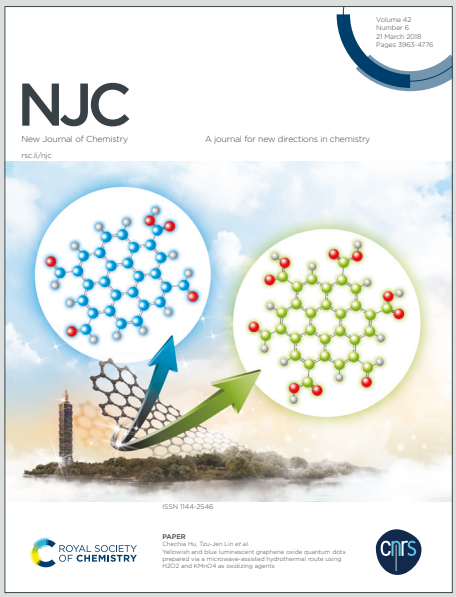


This is an Accepted Manuscript, which has been through the Royal Society of Chemistry peer review process and has been accepted for publication.

Accepted Manuscripts are published online shortly after acceptance, before technical editing, formatting and proof reading. Using this free service, authors can make their results available to the community, in citable form, before we publish the edited article. We will replace this Accepted Manuscript with the edited and formatted Advance Article as soon as it is available.

You can find more information about Accepted Manuscripts in the Information for Authors.

Please note that technical editing may introduce minor changes to the text and/or graphics, which may alter content. The journal's standard Terms & Conditions and the Ethical guidelines still apply. In no event shall the Royal Society of Chemistry be held responsible for any errors or omissions in this Accepted Manuscript or any consequences arising from the use of any information it contains.

View Article Online
DOI: 10.1039/C9NJ04713A

ARTICLE

# Design, Synthesis and Biological Activities of Pyrrole-3-carboxamide Derivatives as EZH2 (Enhancer of Zeste Homologue 2) Inhibitors and Anticancer Agents

Received 00th January 20xx,
Accepted 00th January 20xx

DOI: 10.1039/x0xx00000x

Qifan Zhou[a,†], Lina Jia[b,†], Fangyu Du[a], Xiaoyu Dong[b], Wanyu Sun[b], Lihui Wang[b,**], Guoliang Chen[a,*]

Zeste enhancer homolog 2 (EZH2) is highly expressed in various malignant tumors, which could silence tumor suppressor gene *via* trimethylation of H3K27. Herein was first reported a novel series of pyrrole-3-carboxamide derivatives carrying with pyridone fragment as EZH2 inhibitors. By combining computational modeling, *in vitro* cellular assays and further rational structure-activity relationship exploration and optimization, compound **DM–01** showed powerful inhibition of EZH2. **DM–01** was found to have a significant ability to reduce cellular H3K27me3 level in K562 cells in Western blot test. Meanwhile, our data showed knockdown EZH2 in A549 cells resulted in the decrease of cell sensitivity to **DM–01** at 50 and 100 μM. **DM–01** could also increase the transcription expression of DIRAS3 in a dose-dependent manner, a tumor suppressor in downstream of EZH2, suggesting it was worthy to investigate further as a lead compound.

## 1. Introduction

Disorders in epigenetic regulation, including methylation of DNA and histones, have been recognized as a major feature of malignant tumors. [1] Enhancer zeste of homolog 2 (EZH2), which belongs to a class of methyltransferases, has been found in various malignant cells and is involved in divergent biological processes. [2,3] EZH2 is a catalytic subunit of polycomb repressive complex 2 (PRC2, the other two subunits are VeFS domain containing SUZ12 and WD40 repeat containing protein EED) that acts as a transcriptional repressor. [4] It catalyzes the addition of three methyl groups from the *S*-adenosyl-*L*-methionine (SAM) cofactor to lysine 27 of Histone H3 (H3K27), one of the five main histone proteins involved in the structure of chromatin in eukaryotic cells, which facilitates chromatin compaction and gene silencing of tumor suppressor genes in cancer cells. The functions of EZH2 are closely related to tumor generation, [5] chemotherapy resistance, [6] tumor metastasis, [7,8] and maintain the characteristics of cancer stem cells. [9,10] Subsequent studies have found high expressing EZH2 in a variety of malignancies, including head and neck cancer, bladder cancer, colorectal cancer, and non-small cell lung cancer. [11] Due to this evidence, research on anti-cancer drugs targeting EZH2 has attracted widespread attention.

In recent years, kinds of EZH2 inhibitors with different scaffolds have already been reported. [12] Some of the specific inhibitors of EZH2 have entered clinical trials for the treatment of diffuse large B-cell lymphoma (DLBCL), follicular lymphoma (FL), and SNF5/INI-1/SMARCB1 genetically defined solid tumors, including **GSK–126** (Phase I), [13] **tazemetostat** (**EPZ–6438**, Phase II), [14,15] and **CPI–1205** (Phase I/II) (Fig. 1) [16]. Notably, Epizyme Inc. has submitted a listing application of **tazemetostat** to FDA for treatment for metastatic/locally advanced epithelioid sarcoma in May 2019. More recently, **DS–3201** (**valemetostat**), developed by Daiichi Sankyo, is undergoing Phase I clinical trial. [17,18] **PF–06821497** has been pushed into clinical development by Pfizer for the treatment of adult patients with relapsed or refractory small cell lung cancer (SCLC), castration resistant prostate cancer (CRPC), DLBCL and FL (Fig. 1). [19] Subsequently, **SHR–2554** (structure undisclosed), developed by Jiangsu Hengrui, recently entered phase I clinical trial for the treatment of hematologic-blood cancer. [20] However, there were some defects in the clinical EZH2 inhibitors. For example, **GSK–126** was administered by injection in clinical trials due to its poor pharmacokinetic properties; [21] clinical dose of **tazemetostat** was increased to 800 mg po bid. [22]

To gain insight into the interactions between inhibitors and EZH2 protein, molecular docking simulations were performed (PDB code: 4W2R, [19] Fig. 1). EZH2 inhibitors in clinical trials all have similar and unique pyridone moieties, which are necessary to improve binding to the EZH2 SET domain in SAM-competitive manner *via* forming two hydrogen bonds with $Trp^{521}$. Additional bonding with $Arg^{582}$ or $Tyr^{111}$ is also important. As we known, pyrroles provide access to important subunits and precursors of numerous biologically active compounds, natural products and

[a] *Address here. Key Laboratory of Structure-Based Drugs Design & Discovery of Ministry of Education, School of Pharmaceutical Engineering, Shenyang Pharmaceutical University, No. 103 Wenhua Road, Shenhe District, Shenyang 110016, P.R. China. E-mail addresses: spucgl@163.com (G. Chen).*
[b] *Department of Pharmacology, Shenyang Pharmaceutical University, No. 103 Wenhua Road, Shenhe District, Shenyang 110016, P.R. China*
† Authors contributed equally to this work
Electronic Supplementary Information (ESI) available. See DOI: 10.1039/x0xx00000x

View Article Online
DOI: 10.1039/C9NJ04713A



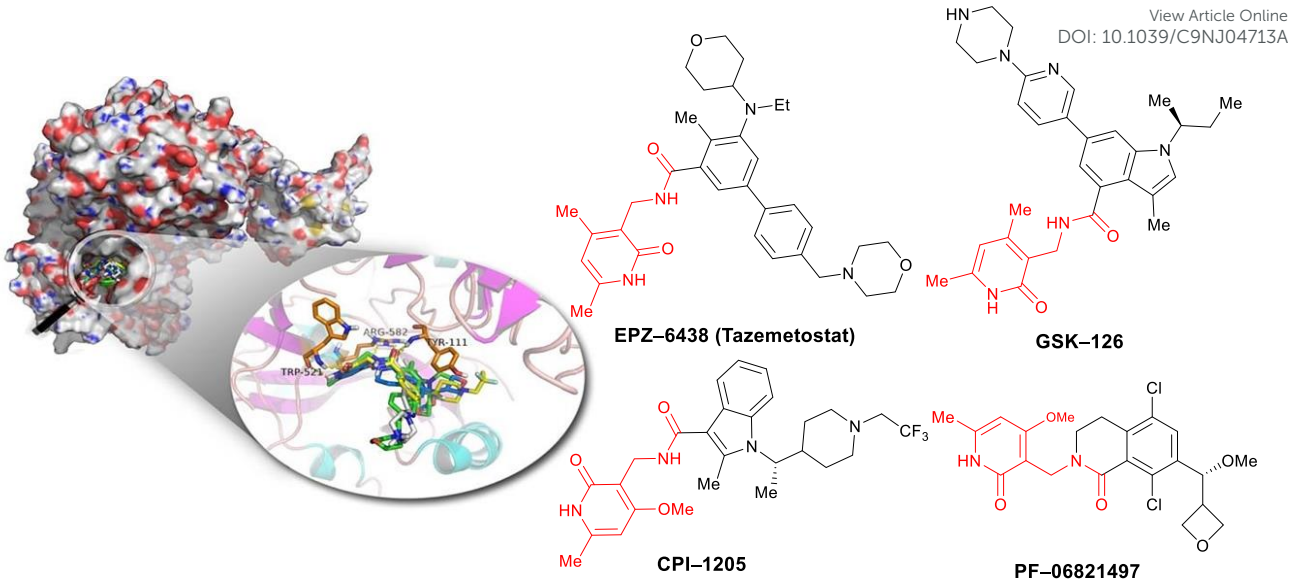


**Fig.1.** Molecular docking model and chemical structures of several clinical EZH2 inhibitors. PDB code: [19] 4W2R; **GSK–126** [13] (white), **tazemetostat** [14] (green), **CPI–1205** [16] (yellow), **PF–06821497** [19] (blue).

pharmaceuticals. [23-25] Due to these evidences, we designed a series of pyrrole-3-carboxamide derivatives according to the biosostere theory using **CPI–1205** as the lead compound (Scheme 1). Compounds **D–01~23** were designed by retaining the two methyl groups adjacent to the pyrrole N, limiting the spatial conformation of *N*-substitutions. Meanwhile, compounds **DM–01~28** were obtained *via* scaffold hopping to find out the effect of the spatial conformation of the *N*-

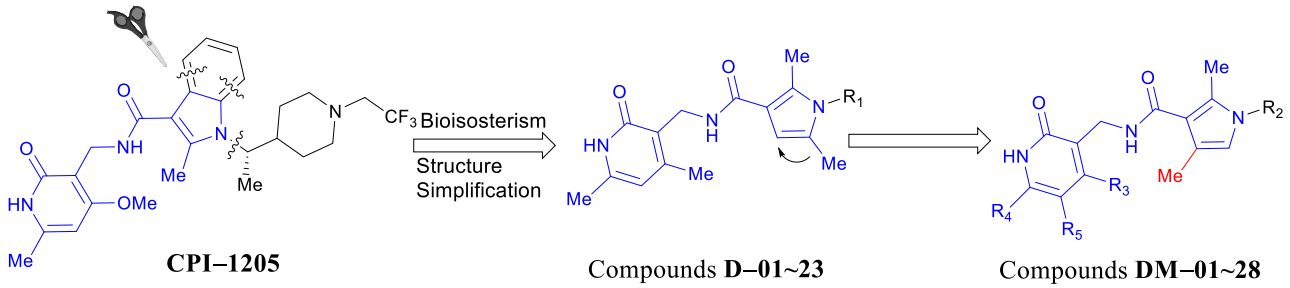


**CPI–1205**
Lead

Compounds **D–01~23**

**D–01;** $R_1$= Bn
**D–02;** $R_1$= 3-OMe-Bn
**D–03;** $R_1$= cyclopropylmethyl
**D–04;** $R_1$= 3,4,5-triOMe-Bn
**D–05;** $R_1$= 4-Br-Bn
**D–07;** $R_1$= 4-Cl-Bn
**D–08;** $R_1$= 3-Cl-Bn
**D–09;** $R_1$= 2-Cl-Bn
**D–10;** $R_1$= 4-F-Bn
**D–11;** $R_1$= 3-F-Bn
**D–12;** $R_1$= 2-F-Bn
**D–13;** $R_1$= 4-triCF$_3$-Bn
**D–14;** $R_1$= 3-triCF$_3$-Bn
**D–15;** $R_1$= 2,4-diCl-Bn
**D–16;** $R_1$= 3,5-diOMe-Bn
**D–17;** $R_1$= 4-OMe-Bn
**D–18;** $R_1$= 2-OMe-Bn
**D–19;** $R_1$= benzo[*d*][1,3]dioxol-5-ylmethyl
**D–20;** $R_1$= 4-Me-Bn
**D–21;** $R_1$= naphthalen-2-ylmethyl
**D–22;** $R_1$= 2-(dimethylamino)ethyl
**D–23;** $R_1$= 2-hydroxyethyl

Compounds **DM–01~28**

**DM–01;** $R_2$= 4-triCF$_3$-Bn, $R_3$=Me, $R_4$=Me, $R_5$=H
**DM–02;** $R_2$= 4-F-Bn, $R_3$=Me, $R_4$=Me, $R_5$=H
**DM–03;** $R_2$= 3-(triCF$_3$, $R_3$=Me, $R_4$=Me, $R_5$=H
**DM–04;** $R_2$= 1-(3,4,5-triOMe-Bn, $R_3$=Me, $R_4$=Me, $R_5$=H
**DM–05;** $R_2$= benzo[*d*][1,3]dioxol-5-ylmethyl, $R_3$=Me, $R_4$=Me, $R_5$=H
**DM–06;** $R_2$= 3,4-diOMe-Bn, $R_3$=Me, $R_4$=Me, $R_5$=H
**DM–07;** $R_2$= 4-Cl-Bn, $R_3$=Me, $R_4$=Me, $R_5$=H
**DM–08;** $R_2$= 3-Cl-Bn, $R_3$=Me, $R_4$=Me, $R_5$=H
**DM–09;** $R_2$= 3-F-Bn, $R_3$=Me, $R_4$=Me, $R_5$=H
**DM–10;** $R_2$= 2-OMe-Bn, $R_3$=Me, $R_4$=Me, $R_5$=H
**DM–11;** $R_2$= 2,4-diCl-Bn, $R_3$=Me, $R_4$=Me, $R_5$=H
**DM–12;** $R_2$= 3-OMe-Bn, $R_3$=Me, $R_4$=Me, $R_5$=H
**DM–13;** $R_2$= 3,5-diOMe-Bn, $R_3$=Me, $R_4$=Me, $R_5$=H
**DM–14;** $R_2$= cyclopropylmethyl, $R_3$=Me, $R_4$=Me, $R_5$=H
**DM–15;** $R_2$= naphthalen-2-ylmethyl, $R_3$=Me, $R_4$=Me, $R_5$=H
**DM–16;** $R_2$= 4-Me-Bn, $R_3$=Me, $R_4$=Me, $R_5$=H
**DM–17;** $R_2$= 4-triCF$_3$-Bn, $R^3$=Me, $R_4$, $R_5$=Cyclohexyl
**DM–18;** $R_2$= 4-triCF$_3$-Bn, $R^3$=H, $R_4$, $R_5$=Cyclopentyl
**DM–19;** $R_2$= 4-triCF$_3$-Bn, $R_3$=Me, $R_4$=Pr, $R_5$=H
**DM–20;** $R_2$= 4-triCF$_3$-Bn, $R^3$=OMe, $R^4$=Me, $R^5$=H
**DM–21;** $R_2$= 4-triCF$_3$-Bn, $R_3$=H, $R_4$=Me, $R_5$=H
**DM–22;** $R_2$= 4-triCF$_3$-Bn, $R_3$=Me, $R_4$= $^i$Pr, $R_5$=H
**DM–23;** $R_2$= 4-triCF$_3$-Bn, $R^3$=H, $R^4$= $^i$Pr, $R^5$=H
**DM–24;** $R_2$= 4-triCF$_3$-Bn, $R^3$=H, $R_4$, $R_5$=Cyclohexyl
**DM–25;** $R_2$= 4-triCF$_3$-Bn, $R^3$=Me, $R^4$=Et, $R^5$=H
**DM–26;** $R_2$= 4-triCF$_3$-Bn, $R^3$=H, $R^4$=Et, $R^5$=H
**DM–27;** $R_2$= 4-triCF$_3$-Bn, $R^3$=H, $R^4$=Me, $R^5$=Me
**DM–28;** $R_2$= 1-(4-(triCF$_3$)phenyl)ethyl, $R_3$=Me, $R_4$=Me, $R_5$=H

**Scheme 1.** Schematic diagram depicting the procedure for the design of the target compounds.

View Article Online
DOI: 10.1039/C9NJ04713A

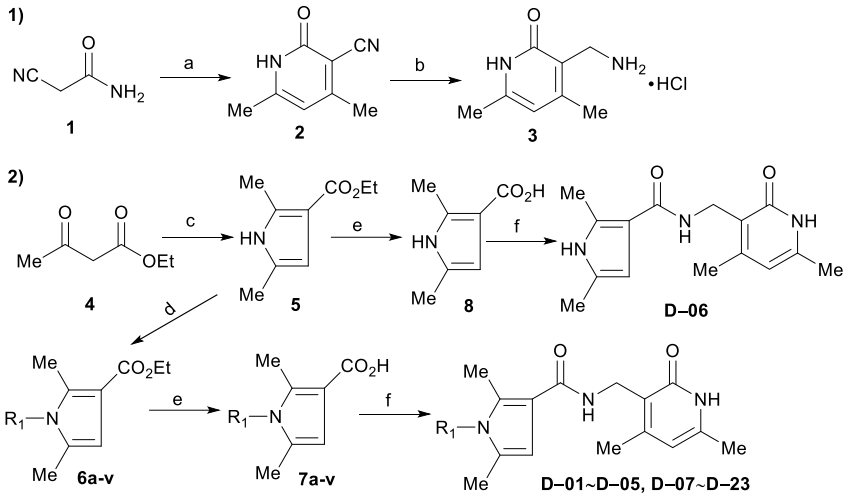


**6a, 7a;** $R_1$= Bn
**6b, 7b;** $R_1$= 3-OMe-Bn
**6c, 7c;** $R_1$= cyclopropylmethyl
**6d, 7d;** $R_1$= 3,4,5-triOMe-Bn
**6e, 7e;** $R_1$= 4-Br-Bn
**6f, 7f;** $R_1$= 4-Cl-Bn
**6g, 7g;** $R_1$= 3-Cl-Bn
**6h, 7h;** $R_1$= 2-Cl-Bn
**6i, 7i;** $R_1$= 4-F-Bn
**6j, 7j;** $R_1$= 3-F-Bn
**6k, 7k;** $R_1$= 2-F-Bn
**6l, 7l;** $R_1$= 4-triCF$_3$-Bn
**6m, 7m;** $R_1$= 3-triCF$_3$-Bn
**6n, 7n;** $R_1$= 2,4-diCl-Bn
**6o, 7o;** $R_1$= 3,5-diOMe-Bn
**6p, 7p;** $R_1$= 4-OMe-Bn
**6q, 7q;** $R_1$= 2-OMe-Bn
**6r, 7r;** $R_1$= benzo[*d*][1,3]dioxol-5-ylmethyl
**6s, 7s;** $R_1$= 4-Me-Bn
**6t, 7t;** $R_1$= naphthalen-2-ylmethyl
**6u, 7u;** $R_1$= 2-(dimethylamino)ethyl
**6v, 7v;** $R_1$= 2-hydroxyethyl

**Reactions and conditions:** (a) Acetylacetone, $K_2CO_3$, $H_2O$, rt; (b) $H_2$/Ni, $NH_4OH$, MeOH, 60 °C; (c) Chloroacetone, $NH_4OH$, 0 °C~rt; (d) Bn-Cls(Brs), NaH, DMF, 0 °C~rt; (e) 1. 60% aq. NaOH, 70 °C; 2. 6 N aq. HCl; (f) **3**, EDCI, HOBt, $Et_3N$, DCM, rt.

**Scheme 2.** Synthetic route to compounds **D–01~D–23**

substitutions and the amide on EZH2 inhibitory activity. All inhibitors contained the key active pyridone fragment, as the previous work showed the modification of this structure was not conducive to activity. [14] Consequently, these derivatives were synthesized and evaluated for their antitumor activities. Their structure-activity relationships were summarized and the mechanism of action that the compounds exerted their EZH2 inhibitory activities was examined by western-blot and computational modeling.

## 2. Results and discussion

### 2.1 Chemistry

The strategy adopted for the synthesis of **D–01~D–23** was outlined in Scheme 2. Briefly, cyanoacetamide **1** was reacted with acetylacetone to obtain 2-cyanopyridone **2**. [14] The cyano group was transferred into amino *via* $H_2$/Ni reduction to afford the key intermediate **3**. Ethyl acetate **4** was reacted with Conc. ammonia which was rapidly followed by a Hantzsch reaction thus forming the desired pyrrole-3-carboxylate **5**. [26] Then **5** was hydrolyzed directly to give pyrrole-3-carboxylic acid **8**. The subsequent condensation of compounds **8** with **3** yielded **D–06**. subsequently Compounds **6a–v** were obtained by reactions of **5** with various halogen substituted materials, which were hydrolyzed to form **7a–v**. The targets **D–01~D–05** and **D–07~D–23** were obtained *via* condensation of **3** with compounds **7a–v**, respectively.

The general synthetic strategy of **DM** series compounds is illustrated as Scheme 3. Initially, pyridinone intermediates **11**~**20** were obtained using ketones and ethyl formates or ethyl acetates as starting materials *via* condensation, [27,28] cyclization and reduction. For another key intermediate **21**, compound **23** was synthesized by condensation of malonylonitrile with 4-methyleneoxetan-2-one in the presence of NaH, [29] which was rapidly followed by rearrangement reaction in the solvents of 4 N HCl under refluxing to form the desired pyridine **24**. Following chlorination and nucleophilic reactions, **24** was assembled to give **26**. The cyano of **26** was transferred to Boc-NH in catalyst system of $H_2$/Raney-Ni/$Boc_2O$/TEA. Finally, **27** was transformed to another pyridinone **21** in the solvents of 4 N HCl under refluxing. Following a Knorr reaction and decarboxylation, *tert*-butyl acetoacetate **28** was assembled to give the key intermediate **30**. [30] Then compound **30** was reacted with several arylmethyl halogens to produce **31a-r**, which was then hydrolyzed and condensed with **3** or **11**~**21** to furnish compounds **DM–01~DM–28**.

### 2.2 *In vitro* biological activity assay and structure-activity relationships

The preclinical data from non-Hodgkin lymphoma (NHL) and selected solid tumors demonstrated that **tazemetostat** inhibit cellular growth *in vitro* and *in vivo*, and reduce H3K27me3 expression, a mark of transcriptional repression. [14] Therefore, our compounds were tested by comparing H3K27me3 protein expression in treated cells with that in un-treated cells through Western Blot. K562 cells (human chronic myeloid leukemia cell) and A549 cells (Human lung adenocarcinoma epithelial cell lines) were used for subsequent studies based on the protein levels of EZH2 and H3K27me3 (Fig. S1).

The Western Blot analysis results on **D** series compounds showed that only **D–16**~**D–19** could inhibit EZH2 at either 5 μM or 10 μM, which resulted in decreased H3K27me3 levels in K562 cells (Fig. S2). However, their ability was much weaker than the positive drug **GSK–126**. A549 cells with stable low expression of EZH2 (A549 sh-EZH2) were established to measure the cell sensitivity toward our compounds by MTT assay (Fig. S3). While A549 sh-EZH2 cells were relatively less sensitive than control cells (A549 sh-EV), which we defined as potential selectivity for EZH2 of candidate compounds. Unfortunately, **D** series

View Article Online
DOI: 10.1039/C9NJ04713A

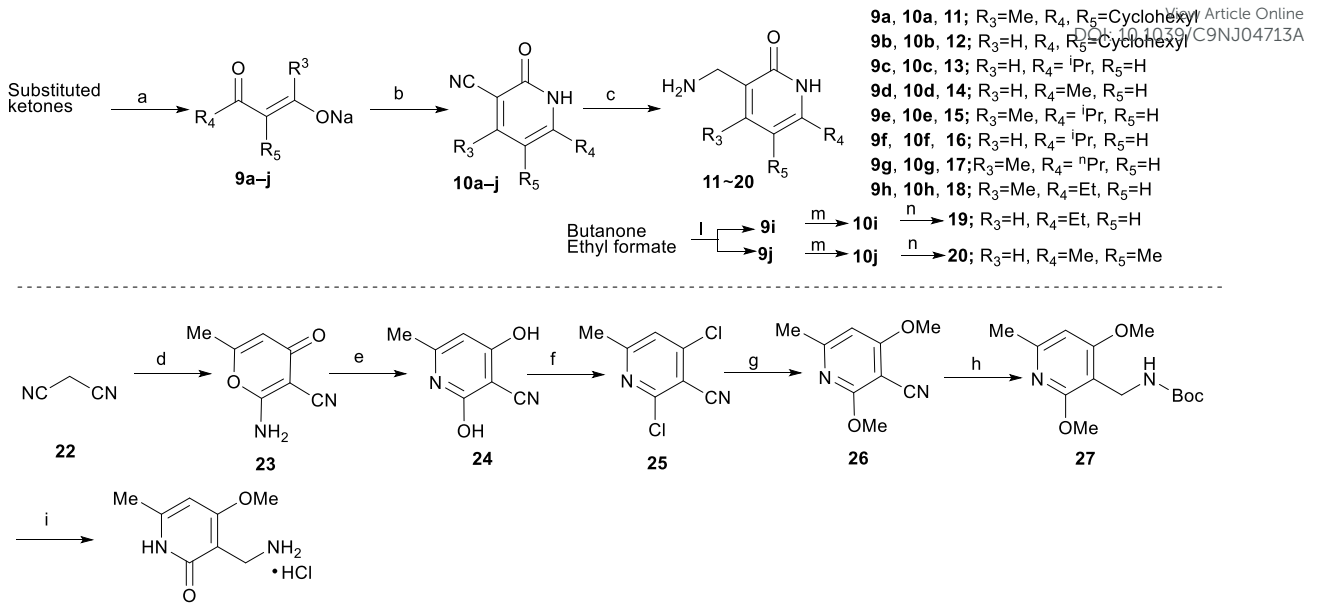





**Reactions and conditions:** (a) Na, $Et_2O$, 0~20 °C, 6 h; (b) 1) Cyanoacetamide, piperidine acetate, r.t.~100 °C, 2 h; 2) 10 N HCl; (c) $H_2$/Ni, MeOH, 25% $NH_4OH$, 60 °C, 11 h; (d) 1) 60% NaH, THF, 0 °C, 0.5 h; 2) 4-Methyleneoxetan-2-one, -10 °C, 1 h; (e) 4 N HCl, reflux, 5 h; (f) $POCl_3$, reflux, 3 h; (g) MeONa, MeOH, reflux, 4 h; (h) $H_2$/Ni, $Boc_2O$, $Et_3N$, MeOH/THF, 30 °C, 48 h; (i) 4 N HCl, reflux, 5 h.

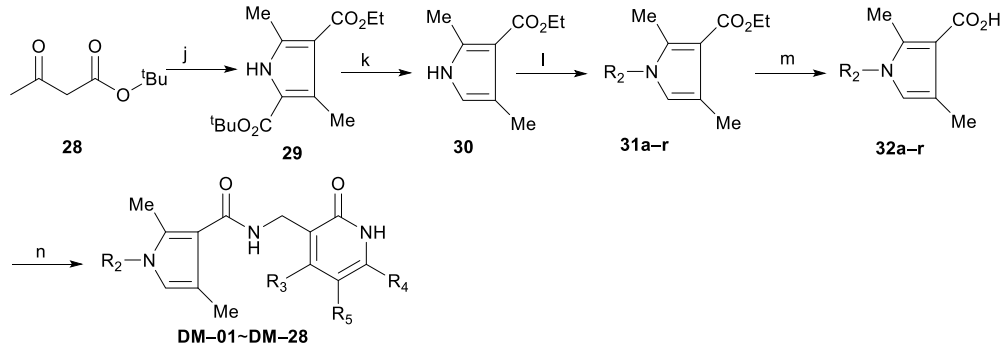


**31a**, **32a;** $R_2$= 4-triCF$_3$-Bn, $R_3$=Me, $R_4$=Me, $R_5$=H
**31b**, **32b;** $R_2$= 4-F-Bn, $R_3$=Me, $R_4$=Me, $R_5$=H
**31c**, **32c;** $R_2$= 3-(triCF$_3$, $R_3$=Me, $R_4$=Me, $R_5$=H
**31d**, **32d;** $R_2$= 1-(3,4,5-triOMe-Bn, $R_3$=Me, $R_4$=Me, $R_5$=H
**31e**, **32e;** $R_2$= benzo[*d*][1,3]dioxol-5-ylmethyl, $R_3$=Me, $R_4$=Me, $R_5$=H
**31f**, **32f;** $R_2$= 3,4-diOMe-Bn, $R_3$=Me, $R_4$=Me, $R_5$=H
**31g**, **32g;** $R_2$= 4-Cl-Bn, $R_3$=Me, $R_4$=Me, $R_5$=H
**31h**, **32h;** $R_2$= 3-Cl-Bn, $R_3$=Me, $R_4$=Me, $R_5$=H
**31i**, **32i;** $R_2$= 3-F-Bn, $R_3$=Me, $R_4$=Me, $R_5$=H
**31j**, **32j;** $R_2$= 2-OMe-Bn, $R_3$=Me, $R_4$=Me, $R_5$=H
**31k**, **32k;** $R_2$= 2,4-diCl-Bn, $R_3$=Me, $R_4$=Me, $R_5$=H
**31l**, **32l;** $R_2$= 3-OMe-Bn, $R_3$=Me, $R_4$=Me, $R_5$=H
**31m**, **32m;** $R_2$= 3,5-diOMe-Bn, $R_3$=Me, $R_4$=Me, $R_5$=H
**31n**, **32n;** $R_2$= cyclopropylmethyl, $R_3$=Me, $R_4$=Me, $R_5$=H
**31o**, **32o;** $R_2$= naphthalen-2-ylmethyl, $R_3$=Me, $R_4$=Me, $R_5$=H
**31p**, **32p;** $R_2$= 4-Me-Bn, $R_3$=Me, $R_4$=Me, $R_5$=H
**31a**, **32a;** $R_2$= 4-triCF$_3$-Bn, $R^3$=Me, $R_4$, $R_5$=Cyclohexyl
**31a**, **32a;** $R_2$= 4-triCF$_3$-Bn, $R^3$=H, $R_4$, $R_5$=Cyclopentyl
**31a**, **32a;** $R_2$= 4-triCF$_3$-Bn, $R_3$=Me, $R_4$=Pr, $R_5$=H
**31q**, **32q;** $R_2$= 4-triCF$_3$-Bn, $R^3$=OMe, $R^4$=Me, $R^5$=H
**31a**, **32a;** $R_2$= 4-triCF$_3$-Bn, $R_3$=H, $R_4$=Me, $R_5$=H
**31a**, **32a;** $R_2$= 4-triCF$_3$-Bn, $R_3$=Me, $R_4$= $^i$Pr, $R_5$=H
**31a**, **32a;** $R_2$= 4-triCF$_3$-Bn, $R^3$=H, $R^4$= $^i$Pr, $R^5$=H
**31a**, **32a;** $R_2$= 4-triCF$_3$-Bn, $R^3$=H, $R_4$, $R_5$=Cyclohexyl
**31a**, **32a;** $R_2$= 4-triCF$_3$-Bn, $R^3$=Me, $R^4$=Et, $R^5$=H
**31a**, **32a;** $R_2$= 4-triCF$_3$-Bn, $R^3$=H, $R^4$=Et, $R^5$=H
**31a**, **32a;** $R_2$= 4-triCF$_3$-Bn, $R^3$=H, $R^4$=Me, $R^5$=Me
**31r**, **32r;** $R_2$= 1-(4-(triCF$_3$)phenyl)ethyl, $R_3$=Me, $R_4$=Me, $R_5$=H

**Reactions and conditions:** (j) 1. $NaNO_2$, HOAc, rt; 2. Ethyl acetoacetate, Zn, 70 °C; (k) 10 N aq. HCl; (l) Substituted benzyl chloride (Br), NaH, DMF, 0 °C~r.t.; (m) 1. 60% aq. NaOH, 70 °C; 2. 6 N aq. HCl; (n) one of **3** or **11~21**, EDCI, HOBt, $Et_3N$, DCM, rt.

**Scheme 3.** Synthetic route to compounds **DM–01~DM–28**

compounds hardly exhibited potential cytotoxicity on either A549 sh-EV cells or A549 sh-EZH2 cells (Table S1).

**DM** series compounds were then obtained *via* transferring the methyl group at pyrrole from C5' to C4' position, in order to produce an angle between the amide and pyrrole relying on the steric hindrance of the two adjacent methyl group (Fig. 2A). Meanwhile, the steric effect of the substituent on the pyrrole-*N* was removed. Western Blot showed that **DM–01~DM–16** could inhibit EZH2 at both two concentrations (5 and 10 μM), which resulted in decreased H3K27me3 levels (Fig. 2B). It was consistent with the result of molecular docking, as shown in Table S2. The DM series compounds and control drugs showed

View Article Online
DOI: 10.1039/C9NJ04713A



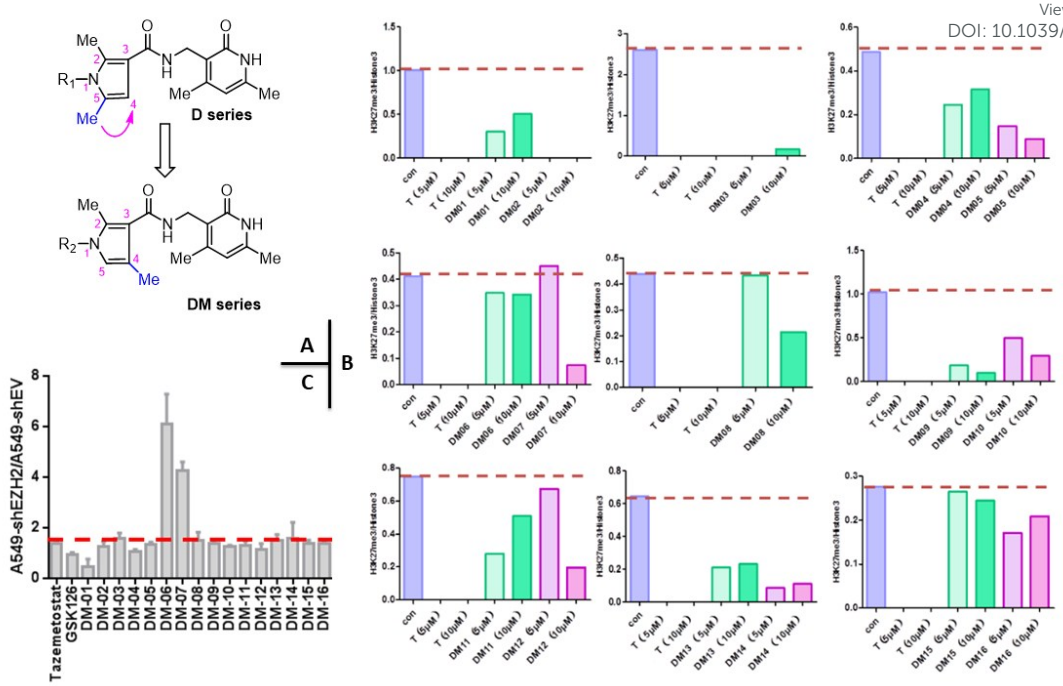


**Fig. 2**. (A) Modified process form **D** to **DM** series compounds; (B) The cell viability of A549 sh-EV and A549 sh-EZH2 cells after **DM** series compounds treatment at 10 μM for 48 h; (C) Western Blot analysis results of H3K27me3 and Histone3 for **DM–01**~**DM–16**.

the better dock scores than that of D series compounds. Thus, it was preliminarily speculated that the methyl group at C4' position of pyrrole was essential for EZH2 inhibitory activity. Notably, **tazemetostat** was used as a positive drug in subsequent experiments as it was proved to be more potent than **GSK–126** in WB analysis. At the concentration of 10 μM, as compared with control cells, A549 sh-EZH2 cells showed less growth inhibition to **DM–01** (Fig. 2C).

It was then investigated the effects of pyrrole-*N* substituents on the cytotoxic activity of **DM** series compounds using MTT assay. For A549 sh-EV cells, compounds with electron-withdrawing substituents (*e.g.*, $-CF_3$, –F) exhibited more

**Table 1.** Antiproliferative activities of compounds **DM–01**~**DM–16**

| Compd. | $IC_{50}$ (μM)±SEM [a] | | | | cLogP [c] |
|---|---|---|---|---|---|
| | A549 sh-EV | A549 sh-EZH2 | Selectivity[b] | K562 | |
| **DM–01** | 72.748±5.45 | 269.7 | 3.7 | 58.706±3.18 | 3.72 |
| **DM–02** | 79.83±7.62 | 47.3±4.85 | 0.6 | > 100 | 2.99 |
| **DM–03** | 43.832±1.66 | 48.8±0.34 | 1.1 | > 100 | 3.70 |
| **DM–04** | > 100 | > 100 | -- | > 100 | 2.46 |
| **DM–05** | 75.978±4.81 | 22.803±0.73 | 0.3 | > 100 | 2.72 |
| **DM–06** | > 100 | > 100 | -- | 64.89±2.28 | 2.47 |
| **DM–07** | > 100 | 64.338±1.43 | -- | 95.415±3.19 | 3.50 |
| **DM–08** | > 100 | > 100 | -- | > 100 | 3.48 |
| **DM–09** | > 100 | 61.924±5.65 | -- | 39.92±1.87 | 2.96 |
| **DM–10** | > 100 | 30.551±1.54 | -- | > 100 | 2.83 |
| **DM–11** | > 100 | 4.902±0.82 | -- | > 100 | 4.11 |
| **DM–12** | 67.66±2.68 | 6.59±0.83 | 0.1 | > 100 | 2.86 |
| **DM–13** | 80.621±6.33 | 10.387±1.53 | 0.1 | > 100 | 2.87 |
| **DM–14** | > 100 | > 100 | -- | > 100 | 2.10 |
| **DM–15** | > 100 | > 100 | -- | > 100 | 4.01 |
| **DM–16** | > 100 | 51.931±3.56 | -- | > 100 | 3.27 |
| **GSK–126** | 16.1±0.054 | 36.3±1.00 | 2.3 | 17.94±1.82 | 3.87 |
| **tazemetostat** | > 100 | > 100 | -- | 59.161±0.55 | 3.45 |

[a] $IC_{50}$: 50% inhibitory concentration (detemined by standard MTT assay for A549, CCK-8 assy for K562). Each experiment was carried out in triplicate. [b] Selectivity = $IC_{50}$ values on A549 sh-EZH2 / A549 sh-EV cells. [c] Octanol-water partition coefficient (LogP) was calculated according to Discovery Studio 3.0.

View Article Online DOI: 10.1039/C9NJ04717A

sufficient cytotoxic effects, such as **DM–01** ($IC_{50}$ = 72.1 μM), **DM–02** ($IC_{50}$ = 79.8 μM) and **DM–03** ($IC_{50}$ = 43.8 μM) depending on $IC_{50}$ values in Table 1. The sequent molecular docking showed that a special H-bond was alternatively formed between the Fluor of the compounds and the target protein, leading to an improving docking score. In contrast, compounds with electron-donating substituents (*e.g.*, –OMe, –Me), particularly substituting at the *para* position, showed much weaker antiproliferative activity with $IC_{50}$ values of over 100 micromolar (**DM–06**, **DM–08**). As compared to **GSK–126** with selectivity index of 2.3, **DM–01** exhibited highly selective for EZH2 with selectivity index of 3.7. Furthermore, **DM–01** also showed comparable inhibitory activity to **tazemetostat** ($IC_{50}$ = 59.2 μM) with an $IC_{50}$ value of 58.7 μM for K562 cells. Besides,

**Table 2.** Antiproliferative activities of target **DM–17**~**DM–31** compounds

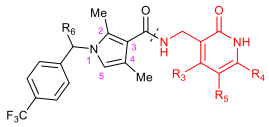

| Compd. | Pyridone Core | $R_6$ | $IC_{50}$ (μM)±SEM [a] K562 | cLogP [b] |
|---|---|---|---|---|
| **DM–17** | 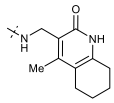 | H | 47.303±2.13 | 1.752 |
| **DM–18** | 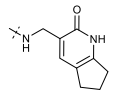 | H | 43.642±1.29 | 3.997 |
| **DM–19** | 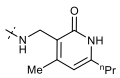 | H | 47.303±1.39 | 4.825 |
| **DM–20** | 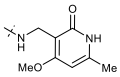 | H | 82.29±1.40 | 3.086 |
| **DM–21** | 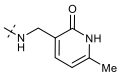 | H | >100 | 3.398 |
| **DM–22** | 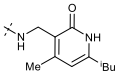 | H | 65.392±1.19 | 5.076 |
| **DM–23** | 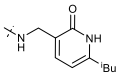 | H | 51.162±1.34 | 4.63 |
| **DM–24** | 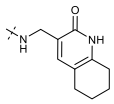 | H | 48.233±1.32 | 4.453 |
| **DM–25** | 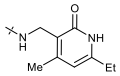 | H | 69.062±1.39 | 4.368 |
| **DM–26** | 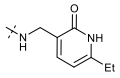 | H | 76.512±2.72 | 3.922 |
| **DM–27** | 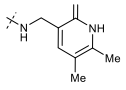 | H | 62.6±2.06 | 3.845 |
| **DM–28** | 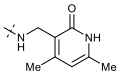 | $CH_3$ | 77.35±1.01 | 4.222 |
| **tazemetostat** | -- | -- | 59.161±0.55 | 3.45 |

[a] $IC_{50}$: 50% inhibitory concentration (detemined by standard CCK-8 assy for K562). Each experiment was carried out in triplicate. [b] Octanol-water partition coefficient (LogP) was calculated according to Discovery Studio 3.0.

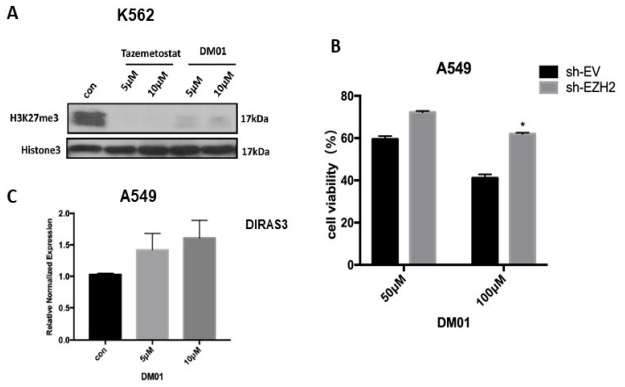


**Fig. 3.** The potency of **DM–01** as a selective EZH2 inhibitor. Cells were treated with **DM–01** (5, 10 μM) for 48 h. (A) The inhibitory effect of **DM–01** on H3K27m3 expression in K562 cells. (B) The cell viability of A549 sh-EV and A549 sh-EZH2. (C) The increasing effect of **DM–01** on DIRAS3 transcription expression in A549 cells.

it was found that **DM–01** had similar cLogP value with positive drugs, ranging from 3~4, indicating a benign Pharmacokinetic property. Further studies showed that **DM–01** strongly inhibited the activity of EZH2 and resulted in abolished H3K27me expression in K562 cells, as depicted in Fig. 3A. Meanwhile, our data showed knockdown EZH2 in A549 cells resulted in the decrease of cell sensitivity to **DM–01** at 50 and 100 μM concentrations (Fig. 3B). Besides, **DM–01** could also increase the transcription expression of DIRAS3 in a dose-dependent manner, a tumor suppressor in downstream of EZH2 (Fig. 3C). The above data suggested that **DM–01** could inhibit tumor growth through suppressing EZH2.

Based on the excellent biological activity results, **DM–01** was further optimized by changing the substitutes of pyridon or benzyl group to obtain its derivatives. Using **tazemetostat** as the positive control, the synthesized targets **DM–17**~**DM–31** were evaluated for the cytotoxic activities *in vitro* against K562 cells, where EZH2 was highly expressed, and the results expressed as $IC_{50}$ values were summarized in Table 2. The activities of most compounds were considerable to that of **tazemetostat**. Fused cycloalkane derivatives **DM–17** ($IC_{50}$ = 47.3 μM), **DM–18** ($IC_{50}$ = 43.6 μM) and **DM–24** ($IC_{50}$= 48.2 μM) slightly improved the inhibitory activities than positive drug, indicating that large hindered substituents were allowed at $R_4$ and $R_5$ positions. It was also confirmed by docking that the modifications in pyridon part was tolerated, sharing similar docking scores with **DM–01** (Table S2). It was also proved that **DM–27** with methyl substitution at R5 position showed its inhibitory with an $IC_{50}$ value of 62.6 μM. However, when the methyl group at $R_3$ position was removed (**DM–21**, $IC_{50} > 100$ μM) or replaced by methoxy (**DM–20**, $IC_{50}$ = 82.3 μM), the inhibitory activity decreased. When methyl was introduced at $R_6$ (**DM–28**), the inhibitory activity decreased with an $IC_{50}$ value 76.5 μM. These results showed that **DM–01** had enough modification space to improve the inhibitory activity.

**2.3 Molecular interactions and docking simulations**

To gain insight into the interactions between our compounds and EZH2 protein, molecular docking simulations were performed (PDB code: 4W2R). Taking **DM–01** as an example,

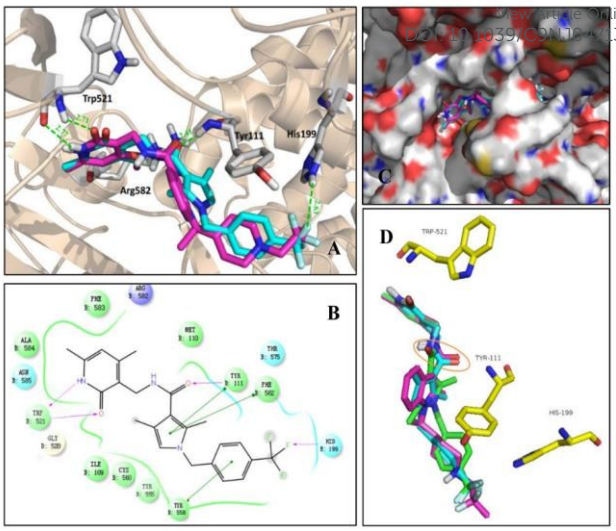


**Fig. 4.** (A) Putative binding modes of **DM–01** (blue) and **CPI–1205** (purple) in 3D representation from molecular docking; Hydrogen bond is shown in green dash lines and small molecules shows as sticks in 3D representation. (B) Ligand 2D interaction diagram for **DM–01** with H-bonds underlined in purple, π–π interactions underlined in green. (C) Surface interaction diagram of **DM–01** (blue) and **CPI–1205** (purple). (D) Structure of **CPI–1205** (purple), **DM–01** (blue) and **D–13** (green) in its active conformation.

the pyridone fragment could form hydrogen bonding with $Trp^{521}$ at distances of 2.71 Å and 2.77 Å, respectively (Fig. 4A and 4C), and another important hydrogen bond interaction with $Tyr^{111}$ was formed at a distance of 2.71 Å. More importantly, **DM–01** could enhance the interaction with receptor *via* binding with $His^{199}$. Additionally, the pyrrole and benzene ring of **DM–01** could also form hydrophobic interactions with $Try^{111}$, $Tyr^{558}$, and $Phe^{562}$ (Fig. 4B). It was obvious that **DM–01** interacted with EZH2 protein in the similar manner with **CPI–1205,** a ligand contained in PDB structure 5LS6 [16]. As described in Fig. 4D, the docking of compounds **D–13**, **DM–01** and **CPI–1205** showed that a same torsional angle between the aromatic ring and the amide carbonyl moiety. However, the amide carbonyl group of **D–13**, an isomer of **DM–01**, faced to reverse direction due to the steric hindrance of methyl group at C3' position, resulting in not able to bind with $Tyr^{111}$. These results explained why the EZH2 inhibitory activities of **D** series compounds were weaker or lost. A field point pattern analysis

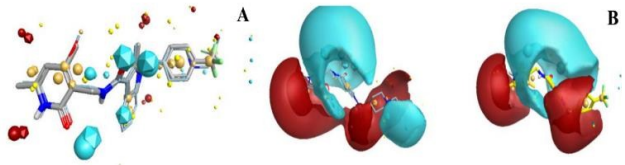


**Fig. 5.** (A) The field point pattern for the conformation of **DM–01** and **CPI–1205**; Negative field points (blue, like to interact with positives/H-bond donors on a protein); Positive field points (red, like to interact with negatives/H-bond acceptors on a protein); Van der Waals surface field points (yellow, describing possible surface/vdW interactions). The size of the point indicates the potential strength of the interaction. (B) The molecular electrostatic potential map at the 0.5 kcal/mol contour of **DM–01** (yellow) and **CPI–1205** (grey); Regions explored in negative electrostatics (blue) and regions explored in positive electrostatics (red).

using this distribution of conformational propensities was also performed (Fig. 5). **DM–01** and **CPI–1205** shared the same negative field points, positive field points and Van der Waals surface field with the similarity value of 0.829 (score was calculated by combining the field score and the shape score). Besides, at the 0.5 kcal/mol contour, **DM–01** and **CPI–1205** have similar negative electrostatics and positive electrostatics in the molecular electrostatic potential map analysis (Fig. 5).

## 3. Experimental

### 3.1 *In vitro* inhibitory activity on A549 sh-EV and A549 sh-EZH2 cells assay

Lentiviruses were produced by transfecting HEK293T cells with shRNA-EZH2-targeting-Plo.k1-plasmids and the helper plasmids pCMV-VSVG, pMDLg-RRE (gag/pol), and pRSV-REV. The cell supernatants were harvested 48 h after transfection. To obtain stable cell lines, A549 cells were infected for 24 h with normal culture medium in the presence of 5 μg/mL of polybrene. After 48 h infection, cells were placed under puromycin selection for one week and then passaged before use. Puromycin was used at 1 μg/ml to maintain A549 cells.

A549 sh-EV and A549 sh-EZH2 cells (MSKCC, USA) plated in RPMI 1640 (Roswell Park Memorial Institute, Gibco) supplemented with 10% FBS (fetal bovine serum, Gibco), and penicillin/streptomycin (HyClone, Shanghai, China) at 37 °C under 5% $CO_2$ until they were 70-80% confluent. The adherent cells were digested with 0.25% trypsin (containing EDTA 1 mmol/L) and suspended in culture medium.

Cell viability was analyzed by using 3-(4,5-dimethyl-2-thiazolyl)-2,5-diphenyl-2-H-tetrazolium bromide (MTT) (Sigmal-aldrich, Shanghai, China), followed by manufacturer's instructions. The Cells were plated in 96-well plate and grown for 24 h. Following the addition of different concentrations (100μM、50μM、10μM、5μM、1μM) of our compounds, the cells were further cultured for 48 h, with 0.5% DMSO as the solvent control group. Then 10 μL MTT regent was added to each well and the culture plate was settled at 37 °C incubation chamber for 3-5 h. The optical density (OD) at a wavelength of 450 nm was detected by using a microplate reader (Molecular Devices, USA). Cell viability was expressed as percentage of untreated controls. Each treatment was performed in triplicate. The half inhibitory concentration $IC_{50}$ values were calculated by IBM SPSS Statistics 21.

### 3.2 Western Blot assay

The human colon cancer cell line K562 cells were incubated in presence of our compounds, **GSK–126** or **tazemetostat** (in 0.5% DMSO) for 24 h, harvested, and rinsed with ice-cold PBS. Total protein extracts were prepared by lysing cells in RIPA buffer 50 mM Tris-HCl, 150 mM NaCl, 0.1% sodium dodecyl sulfate (SDS), 1% NP-40, 0.5% sodium deoxycholate, 1 mM phenylmethylsulfonyl fluoride (PMSF), 100 M leupeptin, and 2 g/mL aprotinin (pH 8.0) supplemented with 0.2 trypsin inhibitory units/ml aprotinin, 0.7 mg/mL pepstatin, and 1 mg/mL leupeptin. An equal amount of total protein extracts from cultured cells were fractionated by 10~15% SDS-PAGE and then electrically transferred onto polyvinylidene difluoride (PVDF) membranes. Mouse or rabbit primary antibodies and appropriate horseradish peroxidase (HRP)-conjugated secondary antibodies were used to detect the designated proteins. The bound secondary antibodies on the PVDF membrane were reacted with ECL detection reagents (Pierce; Rockford, USA) and exposed to X-ray films. Results were normalized to the internal control Histone3 [31,32].

### 3.3 Molecular docking and field points

Molecular docking was performed as previously described. [33] The molecular docking study was performed by AutoDock 4.2.6. The three dimensional structure of EZH2 was retrieved from the Protein Data Bank (PDB code: 4W2R). The binding site was located on the SET region. The 3D structures of **DM–01**, **D–13** and **CPI–1205** were built by using Sybyl-X 2.0. Both the protein and the ligands were prepared by adding polar hydrogen atoms and partial charges with the assistance of AutoDockTools 1.5.6. Grid points were set to 40 at the x, y, z axes. The conformational search was carried out using the Lamarckian Genetic Algorithm. All other parameters were set to default unless stated otherwise. The field point pattern and molecular electrostatic potential map were performed by using Forge 10.4 (Cresset, USA). [34]

## Conclusions

Since EZH2 plays a pivotal role in cell proliferation and survival, it is recognized as one of the significant oncogenic signaling pathways through improving H3K27me3 level. Some of the specific EZH2 inhibitors have entered clinical trials for the treatment of DLBCL, FL, and SNF5/INI-1/SMARCB1 genetically defined solid tumors. Here were first reported a series of pyrrole-3-carboxamide derivatives as EZH2 inhibitors, leading to the discovery of **DM–01** screened by H3K27me3 western blot studies in K562 cells. Combining computational modeling and *in vitro* cellular assays, the structure-activity relationship was summarized. It was found that **DM–01** exhibited its function showing an obvious dependence on EZH2, which was worthy to investigate further as a lead compound. Further development of compound **DM–01** is in progress.

## Conflicts of interest

There are no conflicts to declare.

## Acknowledgements

This work was supported by the project 201602707, 20170540841 (Natural Science Foundation of Liaoning Province), National Natural Science Foundation of China (No. 81572947, 81773216), Scientific Research Fund of Liaoning Provincial Education Department (No. 2017LFW01) and Science Foundation of Shenyang Pharmaceutical University (No. DFJJ2018210).



 

## Notes and references


1 D. Hanahan and R. A. Weinberg, *Cell*, 2011, **144**, 646–674.
2 H. Heyn and M. Esteller, *Cancer Cell*, 2013, **33**, 563–565.
3 J. A. Simon, *Nat. Chem. Biol*., 2012, **8**, 875–876.
4 R. Margueron and D. Reinberg, *Nature*, 2011, **469**, 343–349.
5 W. Cao, R. H. Younis, J. Li, H. Chen, R. Xia, L. Mao, W. Chen and H. Ren, *Cancer Prev. Res*., 2011, **4**, 1816–1824.
6 E. E. Gardner, B. H. Lok, V. E. Schneeberger, P. Desmeules, L. A. Miles, P. K. Arnold, A. Ni, I. Khodos, E. de Stanchina, T. Nguyen, J. Sage, J. E. Campbell, S. Ribich, N. Rekhtman, A. Dowlati, P. P. Massion, C. M. Rudin and J. T. Poirier, *Cancer Cell*, 2017, **31**, 286–299.
7 D. Zingg, J. Debbache, S. M. Schaefer, E. Tuncer, S. C. Frommel, P. Cheng, N. Arenas-Ramirez, J. Haeusel, Y. Zhang, M. Bonalli, M. T. McCabe, C. L. Creasy, M. P. Levesque, O. Boyman, R. Santoro, O. Shakhova, R. Dummer and L. Sommer, *Nat. Commun*., 2015, **6**, 6051–6068.
8 N. Tiwari, V. K. Tiwari, L. Waldmeier, P. J. Balwierz, P. Arnold, M. Pachkov, N. Meyer-Schaller, D. Schübeler, E. van Nimwegen and G. Christofori, *Cancer Cell*, 2013, **23**, 768–783.
9 K. Lund, P. D. Adams and M. Copland, *Leukemia*, 2014, **28**, 44–49.
10 C. J. Chang, J. Y. Yang, W. Xia, C. T. Chen, X. Xie, C. H. Chao, W. A. Woodward, J. M. Hsu, G. N. Hortobagyi and M. C. Hung, *Cancer Cell*. 2011, **19**, 86–100.
11 M. Takawa, K. Masuda, M. Kunizaki, Y. Daigo, K. Takagi, Y. Iwai, H. S. Cho, G. Toyokawa, Y. Yamane, K. Maejima, H. I. Field, T. Kobayashi, T. Akasu, M. Sugiyama, E. Tsuchiya, Y. Atomi, B. A. Ponder, Y. Nakamura and R. Hamamoto, *Cancer Sci.*, 2011, **102**, 1298–1305.
12 H. Ü. Kaniskan and J. Jin, *Curr. Opin. Chem. Biol.*, 2017, **39**, 100–108.
13 A study to investigate the safety, pharmacokinetics, pharmacodynamics and clinical activity of GSK2816126 in subjects with relapsed/refractory diffuse large B cell and transformed follicularlymphoma, http://clinicaltrials.gov/ct2/show/NCT02082977?term=NCT02082977&=1.
14 K. W. Kuntz, J. E. Campbell, H. Keilhack, R. M. Pollock, S. K. Knutson, M. Porter-Scott, V. M. Richon, C. J. Sneeringer, T. J. Wigle, C. J. Allain, C. R. Majer, M. P. Moyer, R. A. Copeland and R. Chesworth, *J. Med. Chem.*, 2016, **59**, 1556–1564.
15 S. K. Knutson, S. Kawano, Y. Minoshima, N. M. Warholic, K. Huang, Y. Xiao, T. Kadowaki, M. Uesugi, G. Kuznetsov, N. Kumar, T. J. Wigle, C. R. Klaus, C. J. Allain, A. Raimondi, N. J. Waters, J. J. Smith, M. Porter-Scott, R. Chesworth, M. P. Moyer, R. A. Copeland, V. M. Richon, T. Uenaka, R. M. Pollock, K. W. Kuntz, A. Yokoi and H. Keilhack, *Mol. Cancer Ther.*, 2014, **13**, 842–854.
16 R. G. Vaswani, V. S. Gehling, L. A. Dakin, A. S. Cook, C. G. Nasveschuk, M. Duplessis, P. Iyer, S. Balasubramanian, F. Zhao, A. C. Good, R. Campbell, C. Lee, N. Cantone, R. T. Cummings, E. Normant, S. F. Bellon, B. K. Albrecht, J. C. Harmange, P. Trojer, J. E. Audia, Y. Zhang, N. Justin, S. Chen, J. R. Wilson and S. J. Gamblin, *J. Med. Chem.*, 2016, **59**, 9928–9941.
17 A Phase 1 Multiple Ascending Dose Study of DS-3201b in Japanese Subjects With Lymphomas, https://clinicaltrials.gov/ct2/show/NCT02732275?term=NCT02732275&rank=1.
18 T. Watanabe, M. Yamagishi, O. Kanno, J. Watanabe, N. Adachi, D. Honma and Y. Hamada, WO 2017/018499A1.
19 P. P. Kung, P. Bingham, A. Brooun, M. Collins, Y. L. Deng, D. Dinh, C. Fan, K. S. Gajiwala, R. Grantner, H. J. Gukasyan, W. Hu, B. Huang, R. Kania, S. E. Kephart, C. Krivacic, R. A. Kumpf, P. Khamphavong, M. Kraus, W. Liu, K. A. Maegley, L. Nguyen, S. Ren, D. Richter, R. A. Rollins, N. Sach, S. Sharma, J. Sherrill, J. Spangler, A. E. Stewart, S. Sutton, S. Uryu, D. Verhelle, H. Wang, S. Wang, M. Wythes, S. Xin, S. Yamazaki, H. Zhu, J. Zhu, L. Zehnder and M. Edwards, *J. Med. Chem.*, 2018, **61**, 650–665.
20 B. Lu, X. D. Shen, M. X. He, D. Liu and M. S. Zhang, WO 2017/084494A1.
21 C. G. Nasveschuk, A. Gagnon, S. Garapaty-Rao, S. Balasubramanian, R. Campbell, C. Lee, F. Zhao, L. Bergeron, R. Cummings, P. Trojer, J. E. Audia, B. K. Albrecht and J-C. P. Harmange, *ACS Med. Chem. Lett.*, 2014, **5**, 378–383.
22 A phase II, multicenter study of the EZH2 inhibitor tazemetostat in adult subjects with INI1-negative tumors or relapsed/refractory synovial sarcoma, https://clinicaltrials.gov/ct2/show/NCT02601950?cond=Tazemetostat&draw=2&rank=11.
23 P. Liu, Y. Yang, Y. Ju, Y. Tang, Z. Sang, L. Chen, T. Yang, Q. An, T. Zhang and Y. Luo, *Bioorg. Chem.*, 2018, **80**, 422–432.
24 G. Meng, C. Liu., S. Qin, M. Dong, X. Wei, M. Zheng, L. Qin, H. Wang, X. He and Z. Zhang, *Res Chem Intermediat.*, 2015, **41**, 8941–8954.
25 G. Tarzia, A. Duranti, A. Tontini, G. Spadoni, M. Mor, S. Rivara, P. V. Plazzi, S. Kathuriac and D. Piomellic, *Bioorgan. Med. Chem.*, 2003, **11**, 3965–3973.
26 Y. Peng, J. Luo, Q. Feng and Q. Tang, *Eur. J. Org. Chem.*, 2016, **2016**, 5169–5179.
27 F. Liu, Y. Y. Hu, D. Li, Q. Zhou and J. M. Lu, *Tetrahedron,* 2018, **74**, 5683–5690.
28 Y. Watanabe, S. C. Shim, T. Mitsudo, M. Yamashita and Y. Takegami, *B. Chem. Soc. Jpn.*, 1976, **49**, 2302–2305.
29 Z. K. Lu and R. J. Twieg, *Tetrahedron*, 2005, **61**, 903-918.
30 G. Meng, C. Y. Liu, S. D. Qin, M. S. Dong, X. M. Wei, M. L. Zheng, L. W. Qin, H. H. Wang, X. S. He and Z. G. Zhang, *Res. Chem. Intermediat.*, 2015, **41**, 1–14.
31 L. Wang, H. Li, Y. Ren, S. Zou, W. Fang, X. Jiang, L. Jia, M. Li, X. Liu, X. Yuan, G. Chen, J. Yang and C. Wu, *Cell Death. Dis.*, 2016, **7**, e2063–2074.
32 L. Wang, G. Chen, K. Chen, Y. Ren, H. Li, X. Jiang, L. Jia, S. Fu, Y, Li, X. Liu, S. Wang, J. Yang and C. Wu, *Oncotarget*, 2015, **6**, 9740–9755.
33 Q. Zhou, C. Peng, F. Du, L. Zhou, Y. Shi, Y. Du, D. Liu, W. Sun, M. Zhang and G. Chen, *Eur. J. Med. Chem.*, 2018, **151**, 39–50.
34 T. Cheeseright, M. Mackey, S. Rose and J. G. Vinter, *Expert. Opin. Drug Discov.*, 2007, **2**, 131–144.

View Article Online
DOI: 10.1039/C9NJ04713A



## Graphical Abstract

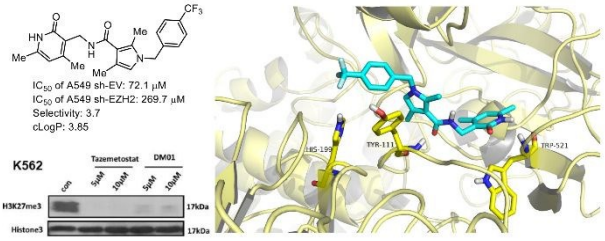


## Highlight

A series of pyrrole-3-carboxamide derivatives targeting on EZH2 were designed and synthesized.

Compound **DM–01** was found to possess significant inhibitory activities to reduce cellular H3K27me3 level in K562 cells.

The structure–activity relationships of the synthesized compounds were summarized.

Molecular docking studies were performed.